

www.acsami.org Research Article

Slot-Die-Coated Ternary Organic Photovoltaics for Indoor Light Recycling

Mahmoud E. Farahat, Audrey Laventure, Michael A. Anderson, Mathieu Mainville, Francesco Tintori, Mario Leclerc, Erin L. Ratcliff,* and Gregory C. Welch*



Cite This: https://dx.doi.org/10.1021/acsami.0c11809



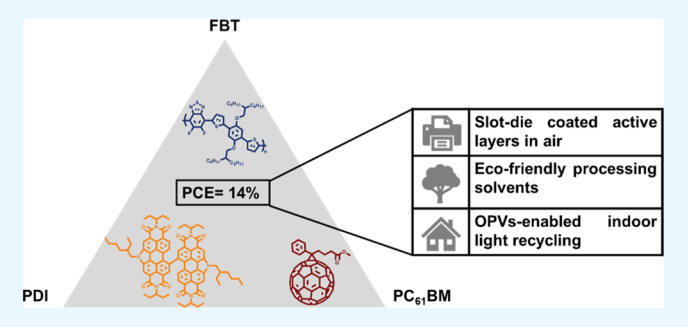
ACCESS I

III Metrics & More

Article Recommendations

s Supporting Information

ABSTRACT: Efficient organic photovoltaics (OPVs) based on slot-die-coated (SD) ternary blends were developed for low-intensity indoor light harvesting. For active layers processed in air and from eco-friendly solvents, our device performances (under 1 sun and low light intensity) are the highest reported values for fluoro-dithiophenyl-benzothiadiazole donor polymer-based OPVs. The N-annulated perylene diimide dimer acceptor was incorporated into a blend of donor polymer (FBT) and fullerene acceptor (PC $_{61}$ BM) to give ternary bulk heterojunction blends. SD ternary-based devices under 1 sun illumination showed enhanced power conversion efficiency (PCE) from 6.8 to 7.7%. We observed



enhancement in the short-circuit current density and open-circuit voltage of the devices. Under low light intensity light-emitting device illumination (ca. 2000 lux), the ternary-based devices achieved a PCE of 14.0% and a maximum power density of 79 μ W/cm² compared to a PCE of 12.0% and a maximum power density of 68 μ W/cm² for binary-based devices. Under the same illumination conditions, the spin-coated (SC) devices showed a PCE of 15.5% and a maximum power density of 88 μ W/cm². Collectively, these results demonstrate the exceptional promise of a SD ternary blend system for indoor light harvesting and the need to optimize active layers based on industry-relevant coating approaches toward mini modules.

KEYWORDS: indoor light harvesting, organic photovoltaics, slot-die coating, halogen-free processing, perylene diimide, PPDT2FBT

■ INTRODUCTION

Indoor photovoltaics (iPVs) target the harvesting of artificial light and are expected to play a vital role as a power supply source for internet of things (IoT) systems. One immediate market entry point for iPV is powering small electronic devices, as tens of billions of these devices are expected to be installed within the coming decade. Indoor light intensities in the range of 500 lux (office spaces) and 1000 lux (factories) are sufficient to provide > 100 μ W power when using small iPV modules. This power is enough to operate smart IoT devices such as radio frequency identification tags (\sim 10 μ W), smart thermostats (\sim 18 μ W), and passive WiFi (\sim 60 μ W). ¹⁻⁴ Hence, there is a need for efficient and low-cost iPVs that can be effectively integrated with those IoT-based devices. Critical to iPV deployment are the following: (i) band gap engineering of the active layer—employing photoactive materials with medium band gaps (visible range light absorption) to match the emission of light-emitting device (LED) lighting; (ii) high open-circuit voltage (V_{oc}) values to offset the voltage loss under low light intensity; 3,5 and (iii) vetting device performance at scale.

To the first point, various photoactive materials lend feasibility toward iPVs, including dye-sensitized, perovskite, and organic semiconductors. Of these, organic photo-

voltaics (OPVs) stand out as a promising candidate for indoor light recycling applications for a few reasons. In terms of feasibility, the power conversion efficiency (PCE) of OPV devices has reached a very high value of 18% for a single junction under 1 sun illumination (AM 1.5G, 100 mW/cm²). OPVs have active layers constructed from organic chromophores with high extinction coefficients in the visible region of the electromagnetic spectrum (i.e., overlapping with the emission spectra of artificial indoor lights). OPVs can be easily solution processed from halogen-free solvents 14,15 onto lightweight substrates 16 and adapted to a variety of form factors. 17 OPVs have a high compatibility with various coating techniques such as blade coating and slot-die coating which is favorable for large-scale manufacturing. 18-20 Compared to inorganic photovoltaics, OPVs have lower PCEs under 1 sun illumination. However, because of a highly tunable optical absorption and small current leakage under low light

Received: June 29, 2020 Accepted: September 4, 2020



intensities, OPVs have shown excellent performance in harvesting indoor light energy, more so than inorganic-based technologies.^{3,21} Small current leakage can enable thicker active layers with a higher fill factor (FF) which is crucial for large-scale production.²² Because of the low impact of series resistance on the performance of OPVs under dim lights, replacement of the common ITO electrode becomes feasible enabling the use of lower cost and sustainable transparent conducting electrodes.^{5,23}

Given these promising attributes, much progress toward indoor OPVs (iOPVs) has been made and, as such, has recently been highlighted.²² Briefly, under low light intensity LED illumination, OPV devices have been reported with PCEs over 15%.²¹ Hou and co-workers reported a OPV device with a champion PCE of 26% under 1000 lux LEDs, achieved through rational materials design meeting iOPV criteria.²⁴ Proof-of-concept iOPVs have been established for charging of a super-capacitor and wireless sensor nodes. 25,26 Despite this, the performance of OPV devices under indoor light illumination is still far from the theoretical maximum PCE values (~51-57%),²⁷ warranting further investigation and optimization. What is needed is an increase in V_{oc} approaching or exceeding 1 V and a more concerted focus on band gap engineering to match the full indoor LED emission spectrum. We emphasize that this should be done in parallel with toscale, air-compatible processing methods that utilize green solvents to keep costs low and be human and environment

A promising materials system developed to achieve the desired metrics has recently been introduced by the Woo research team. A binary blend system composed of the semicrystalline poly[(2,5-bis(2-hexyldecyloxy) phenylene)-alt-(5,6-difluoro-4,7-di(thiophen-2-yl)benzo[c][1,2,5]thiadiazole)] (PPDT2FBT, herein referred to as FBT) polymer and [6,6]-phenyl-C71-butyric acid methyl ester (PC₇₁BM) fullerene gave OPV device with a PCE of 9%, with thick active layers (~300 nm), and exhibited a high thermal stability.²⁸ The active layer was readily processed via slot-die coating—a roll-to-roll compatible technique—resulting in a device PCE of 7.5% under 1 sun.²⁹ Evaluation under LED illumination (1000 lux) showed a PCE increase to 16%.³⁰ Because of the high thermal stability, thickness tolerance, and strong visible light absorption, we envisioned that this FBT:fullerene photoactive layer is a reliable candidate for iOPV construction and further enhancement using the ternary blend approach.³¹ Specifically, ternary blends have been used as a successful strategy for enhancing device photocurrent generation through better spectral matching, increasing the device $V_{\rm oc} \geq 1~{
m V}$ via energy cascading to minimize loss processes, and controlling active layer morphology for enhanced transport over recombination. 32-35 A ternary approach has been investigated and proved to be promising for indoor light harvesting. 36-38 It was therefore suggested to apply this strategy to the FBT:fullerene system to further enhance device performance.

The Welch research group has extensively investigated the use of the N-annulated perylene diimide dimer $\rm tPDI_2N\text{-}EH$ (PDI) as a non-fullerene acceptor (NFA) in both binary $^{39-42}$ and ternary 43 OPVs. Devices based on FBT:PDI [active layers slot-die coated (SD) from o-xylene] exhibited high $V_{\rm oc}$ values of 1.02 and 0.84 V under 1 sun and 1000 lux illumination, respectively, with PCEs of 4 and 9% in each case. 44 In contrast, OPVs with FBT:PC61BM active layers had PCEs of 8 and 14%

under 1 sun and 1000 lux illumination, respectively, but with $V_{\rm oc}$ values of 0.78 V or less. ⁴⁴ Inspired by the result that PDI could significantly raise the $V_{\rm oc}$ of PBDB-T:PC₆₁BM-based OPVs when used as a third component, ^{43,45} we hypothesized that ternary blends of FBT:PC₆₁BM:PDI could deliver OPVs with both high $V_{\rm oc}$ and PCE and have utility as indoor light recycling devices.

Herein, we report on inverted-type ternary OPV devices with FBT:PC₆₁BM:PDI active layers processed from a halogen-free solvent mixture [o-xylene and 1% (v/v) panisaldehyde (AA)]⁴⁶ in air via two different coating techniques (spin coating and slot-die coating). All ternary blends were fabricated with the same donor/acceptor ratio (1:1.5 w/w) and 20 mg/mL total concentration. It was found that increasing the weight percentage of PDI in the ternary blend up to 20% (1:1.2:0.3) simultaneously enhances both device short-circuit current (J_{sc}) and V_{oc} although a small decrease in the FF is observed. A fraction of 20% was found to be the optimum PDI content in the ternary blend. For spincoated (SC) active layers, improved PCEs of 7.9% for the ternary blend from 7.0% for the binary were obtained. For active layer processing carried out using slot-die coating (SD), PCEs of 7.7% for ternary blend compared to 6.8% for binary blend were achieved. Under low light intensity using LED illumination (2000 lux), the SD ternary devices showed PCEs of 14.0% compared to 12.0% for the binary. The SC ternary devices fabricated from synthetically optimized FBT batches showed PCEs of 15.5% compared to 13.1% for the binary under the same illumination conditions. The stability of the SD ternary devices has also been examined under ambient conditions and thermal stress showing stable device performance. With a $V_{\rm oc}$ increase due to PDI incorporation and $V_{\rm oc}$ loss < 170 mV under low light intensity, the FBT:PC₆₁BM:PDI ternary system proves to be a potential candidate for successful SD iOPVs. This opens a promising avenue of research and practical application for ternary blend OPVs.

■ EXPERIMENTAL SECTION

Material and Solutions Preparation. The polymer FBT was provided by Brilliant Matters ($M_{\rm n}=39~{\rm kg/mol}$ and $M_{\rm w}=82~{\rm kg/mol}$) and our collaborator at Université Laval ($M_{\rm n}=40~{\rm kg/mol}$ and $M_{\rm w}=88~{\rm kg/mol}$). PC₆₁BM was purchased from Ossila. tPDI₂N-EH (PDI) was synthesized as previously report. The FBT and PC₆₁BM blend (1:1.5 w/w and total concentration of 20 mg/mL) were dissolved in o-xylene with 1% (v/v) AA as solvent additive. PDI was added as a third component to form the ternary system (FBT/PC₆₁BM/PDI) with weight ratios of (1:1.35:0.15), (1:1.2:0.3), (1:1.05:0.45), (1:0.9:0.6), and (1:0.75:0.75). All solutions were based on o-xylene containing 1% AA (v/v). All solutions were heated at 60 °C with continuous stirring in air overnight prior to device fabrication. ZnO precursor solutions were prepared following the solgel method proposed by Sun et al. PEIE (polyethylenimine ethoxylated) (35–40 wt % in water) was prepared with a final concentration of 0.1 wt % in 2-methoxyethanol.

Device Fabrication. An inverted-type device architecture of glass/ITO/ZnO or (ZnO/PEIE)/active layer/MoO $_x$ /Ag was used. Devices were fabricated using ITO-coated glass substrates cleaned by sequentially ultrasonicating with detergent and deionized water, acetone, and isopropanol followed by UV/ozone cleaning for 30 min. The room-temperature solution containing the ZnO solution was SC at 4500 rpm and then annealed at 200 °C in a purge box for 30 min. A solution of 0.1 wt % PEIE in 2-methoxyethanol was SC over the ZnO layer at 5000 rpm followed by substrate annealing at 110 °C for 10 min. For SC devices, the active layer solution was coated at room temperature at different spin speeds for 60 s. For SD devices, the

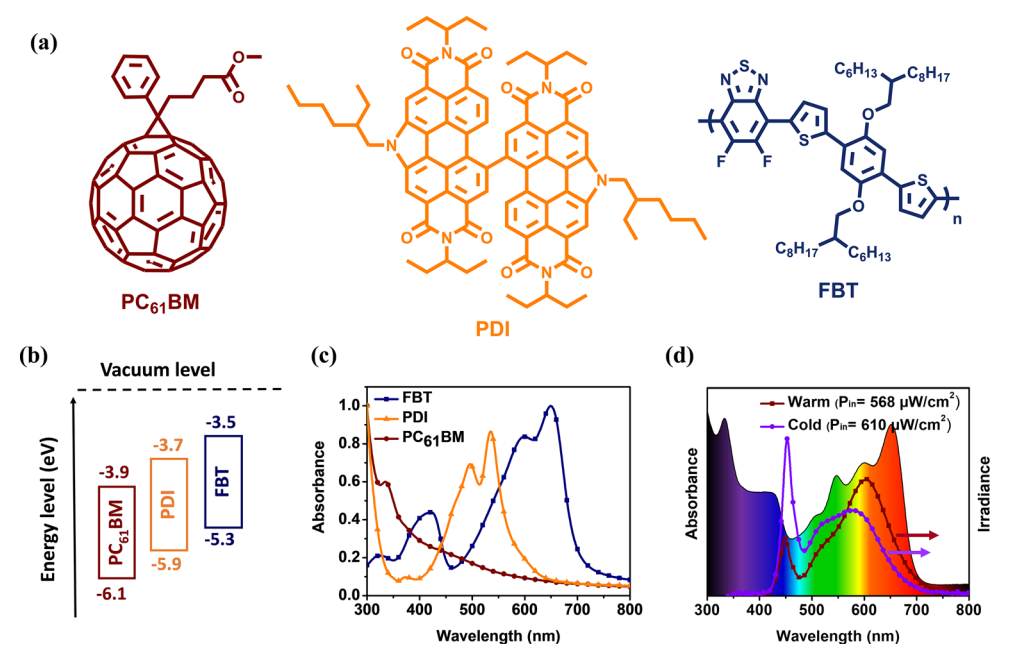


Figure 1. (a) Chemical structures of organic materials used in the study, (b) electronic energy levels determined by cyclic voltammetry, (c) optical absorption spectra of the neat films SC from o-xylene (10 mg/mL), (d) emission spectra of a 2700 K (warm) and 6500 K (cold) at 2000 lux LED illumination with the optical absorption spectrum of the SC ternary blend [FBT/PC $_{61}$ BM/PDI (1:1.2:0.3)] from a 20 mg/mL in o-xylene solution [containing 1% (v/v) AA] superimposed to show the match between the emission spectra of the LEDs and the absorption spectrum of the ternary blend.

active layer solution was coated on top of the ZnO/PEIE bilayer using a compact sheet coater from FOM Technologies equipped with a 13 mm wide slot-die head using a solution dispense rate of 25 $\mu L/\text{min}$ and a substrate motion speed of 20 cm/min. The substrates with the cast active layers [thicknesses ranging from 80 to 100 nm, determined via atomic force microscopy (AFM)] were kept in a nitrogen-filled glovebox overnight before evaporating 10 nm MoO $_x$ and 100 nm Ag under 1 \times 10 $^{-5}$ Torr. The active area of the devices was defined by a shadow mask (0.14 cm 2).

Device Characterization. Optical absorption spectra were recorded using an Agilent Technologies Cary 60 UV-vis spectrometer at room temperature. AFM images were acquired using a TT-2 AFM (AFM Workshop, USA) in the tapping mode and WSxM software with a 0.01–0.025 Ω /cm Sb (n)-doped Si probe with a reflective back side aluminum coating. Photoluminescence (PL) spectra were recorded using an Agilent Technologies Cary Eclipse fluorescence spectrophotometer at room temperature. The current density-voltage (J-V) curves were measured by a Keithley 2420 source measure unit. The photocurrent was measured under AM 1.5 illumination at 100 mW/cm² (Newport 92251A-1000 Solar Simulator). The standard silicon solar cell (Newport 91150V) was used to calibrate light intensity. External quantum efficiency (EQE) was measured in a QEX7 Solar Cell Spectral Response/QE/IPCE Measurement System (PV Measurement, model QEX7, USA) with an optical lens to focus the light into an area about 0.04 cm², smaller than the cell. The silicon reference cell was used to calibrate the EQE measurement system in the wavelength range from 300 to 1100 nm. For indoor testing, a Coidak bulb was used as the illumination source. The P_{in} was measured involving a Newport Si-photodiode (818-SL/ DB, 1 cm² area) connected to an Ossila XTralien X200 source measure unit. The illuminance was measured using a commercial digital luxmeter (Dr Meter). The values are reported in Table S3. The illuminance at which the OPV devices were tested can also be calculated using the Si-photodiode response. More details can be found in the Supporting Information (Figures S6-S8 and Tables S3-S5). For the light-soaking step, devices were kept for 30 s under AM 1.5 illumination at 100 mW/cm² (Newport 92251A-1000 Solar Simulator), then directly measured under different indoor light intensities (ca. 2000, 1000, and 400 lux). The power and light

intensities of both 1 sun and low light were calibrated using a standard monosilicon solar cell (Oriel, model 91150V, Newport).

Grazing Incidence Wide-Angle X-ray Scattering. Grazing incidence wide-angle X-ray scattering (GIWAXS) experiments were carried out on beamline 11-3 at the Stanford Synchrotron Radiation Lightsource (SSRL), equipped with a two-dimensional (2D) Rayonix MX225 CCD area detector. The incident angle of measurement was $\sim\!0.11-0.12^\circ$, and the beam energy was maintained at 12.7 keV. A LaB6 standard sample was used to calibrate the wavelength and sample-detector distance. The obtained 2D images were converted from intensity versus pixel position to intensity versus reciprocal space (q-space) using WAXS tools and Nika macros in Igor 6.37. 2D images were reduced to one-dimensional (1D) intensity versus q_z - and q_{xy} - space by integration of cake segments taken from chi of $0-15^\circ$ and $73-88^\circ$, respectively. 50

■ RESULTS AND DISCUSSION

Materials Selection. The ternary blend system consists of FBT as the electron donor polymer, PC61BM as the fullerene electron acceptor, and the PDI as the NFA third component. Figure 1a shows the chemical structures of these materials. Figure 1b shows the energy levels, determined from the $E_{1/2}$ values of the solution-based cyclic voltammetry, and the relative energetic alignment between FBT, PDI, and PC₆₁BM. The neat material energetics predict suitable energy cascades for ternary blends, with approximately 200 mV offsets in lowest-unoccupied molecular orbitals to drive electron transfer. The optical absorption spectra of the neat films of these three compounds are shown in Figure 1c. The materials were chosen in part to cover a broad region of the indoor LED emission spectrum. PDI has strong optical absorption from 400 to 650 nm which complements that of FBT (450-750 nm). The optical absorption spectra of both FBT and PDI overlap with the emission spectrum of the artificial white LEDs (400-650 nm) indicating that the ternary blend is expected to effectively absorb the photons in this

range, as shown in Figure 1d. Control OPV devices based on the binary blends (FBT:PDI and FBT:PC61BM, Table S1 and Figure S1) were fabricated and gave values similar to our previous finding.4

Ternary Blend Optimization. The first processing strategy was to optimize the blend formulation, independent of the contacts, which will be described below. Figure 2a shows

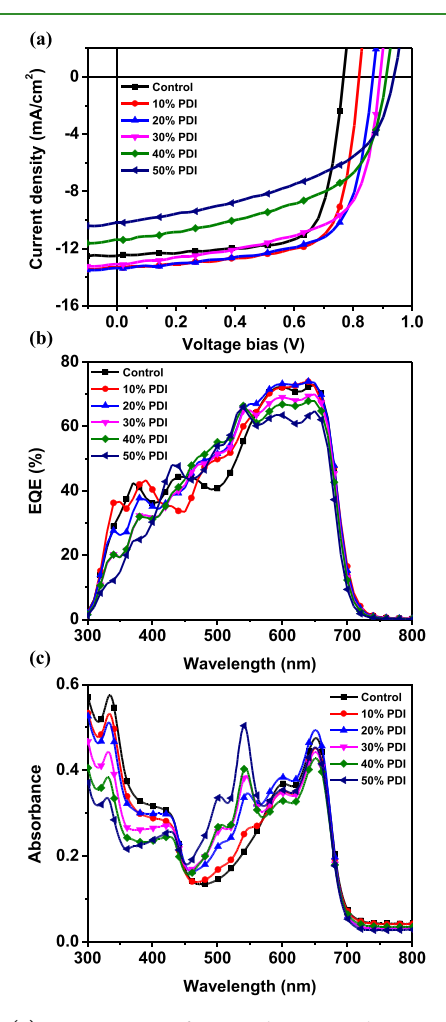


Figure 2. (a) J-V curves of OPV devices with SC active layers containing different PDI % in the ternary system under 1 sun illumination, (b,c) are the corresponding EQE and UV-vis optical absorption spectra, respectively. The control device corresponds to the binary FBT:PC61BM system.

J-V curves of the SC devices with different PDI % in the ternary blend (FBT:PC61BM:PDI) compared to the binary blend (FBT:PC₆₁BM, referred to as the control device). Inverted architecture (glass/ITO/ZnO/active layer/MoO_x/ Ag) was used for the device fabrication with all active layers air-processed from the halogen-free solvent mixture [o-xylene + 1% (v/v) AA]. After careful optimization of the additives based on the device performance of the binary systems (Figure S1 and Table S1), we decided to replace diphenyl ether, which was reported in our previous study, with AA, because this additive is not only considered green but has shown to improve the morphology of $PC_{61}BM$ -based active layers. ⁵¹ The control devices based on the binary blend (FBT:PC₆₁BM) achieved a maximum PCE of 7.0% with the following photovoltaic parameters ($J_{sc} = 12.5 \text{ mA/cm}^2$, $V_{oc} = 0.76 \text{ V}$,

and FF = 73%), as shown in Table 1. PDI was added in different percentages (10-50%) to FBT:PC₆₁BM maintaining

Table 1. Photovoltaic Metrics of OPV Devices with SC Active Layers Containing Different PDI % in the Ternary Blend System under 1 sun Illumination

FBT:PC ₆₁ BM:PDI ^{a,b}	$V_{\rm oc} (V)^c$	$J_{\rm sc}$ $({\rm mA/cm^2})^c$	FF (%) ^c	PCE (%) ^c
control (1:1.5:0)	0.76 (0.76)	12.5 (12.4)	73 (73)	7.0 (7.0)
10% PDI (1:1.35:0.15)	0.82 (0.82)	13.3 (13.2)	71 (70)	7.7 (7.6)
20% PDI (1:1.20:0.30)	0.86 (0.86)	13.4 (13.2)	68 (68)	7.9 (7.8)
30% PDI (1:1.05:0.45)	0.88 (0.88)	13.1 (12.5)	63 (63)	7.3 (7.0)
40% PDI (1:0.90:0.60)	0.90 (0.90)	11.4 (11.0)	54 (54)	5.6 (5.4)
50% PDI (1:0.75:0.75)	0.93 (0.93)	10.2 (9.8)	49 (48)	4.7 (4.4)

^aDevice architecture: glass/ITO/ZnO/active layer/MoO_x/Ag. ^bDevices processed from o-xylene containing 1% AA additive, 20 mg/mL total concentration, and (1:1.5) D:A1:A2 ratio [D: FBT (supplied by Brilliant Matters), A₁: PC₆₁BM, and A₂: PDI]. ^cThe values of the best device are reported, while the values in the parentheses stand for the average PCEs from over 15 devices with 0.14 cm² active area. Standard deviation of the PCE values are presented in Figure S2a.

a total donor/acceptor ratio of 1:1.5 (w/w) and a 20 mg/mL total concentration for all blend solutions. Increasing the percentage of PDI in the ternary blend up to 20% (1:1.2:0.3) simultaneously enhanced both J_{sc} and V_{oc} (Table 1 and Figure 2a). The optimum PDI % was found to be 20% (1:1.2:0.3) which delivered a maximum PCE of 7.9% with the following photovoltaic parameters ($I_{sc} = 13.4 \text{ mA/cm}^2$, $V_{oc} = 0.86 \text{ V}$, and FF = 68%), showing a 100 mV increase in V_{oc} compared to the

EQE (Figure 2b) combined with the optical absorption spectra (Figure 2c) confirms the contribution of PDI to the photocurrent generation within the ternary devices over the 400-650 nm absorption range, which is consistent with the enhanced J_{sc}. Further increasing the PDI to 40% (1:0.9:0.6) adversely affected J_{sc} (11.4 mA/cm²) and FF (54%) while still increasing the $V_{\rm oc}$ (0.90 V) yielding an overall lower PCE of 5.6%. This deterioration in device performance is expected with increasing PDI % in the ternary blend owing to the lower electron mobility of PDI (ranges from $\times 10^{-6}$ to $\times 10^{-7}$ cm² V⁻¹ $(s^{-1})^{48,52}$ compared to PC₆₁BM (×10⁻⁴ cm² V⁻¹ s⁻¹),⁵³ and no major changes to the surface morphology or PL quenching were observed, implying a similar morphology (AFM height images in Figure S3 and PL in Figure S4). On the other hand, the hole mobility of FBT polymer donor was reported to be 1.4×10^{-4} cm² V⁻¹ s^{-1.54} The large mismatch between the electron and hole mobilities of PDI dimer and FBT polymer donor might explain the reason behind the drop in the FFs. Overall, these data confirm that the PDI can boost device $V_{
m oc}$ while maintaining a high device PCE value.

Slot-Die Coated Active Layers. As a further optimization step, a ZnO/PEIE bilayer was tested as an electron transport layer (ETL) in order to enhance the device performance, reproducibility, and stability.⁵⁵ The SC active layers of the optimized ternary blend were used to determine the effect of PEIE on the device performance. The ZnO/PEIE bilayer exhibited better device performance and consistency compared to the ZnO only layer (a detailed comparison between ZnO and ZnO/PEIE-based devices is provided in Table S2 and Figure S5). The optimized ternary conditions (20 wt % PDI) and the FBT:PC61BM binary blends were fabricated using slotdie coating and the optimized ZnO/PEIE bilayer as the ETL.

Under 1 sun illumination, the SD ternary devices yielded a PCE of 7.7% with the following photovoltaic parameters (I_{sc} = 13.0 mA/cm², $V_{oc} = 0.86$ V, and FF = 69%) compared to 6.8% with the following photovoltaic parameters ($J_{sc} = 12.3 \text{ mA/}$ cm², $V_{oc} = 0.78$ V, and FF = 71%) for the binary counterparts. Optimized SC ternary and binary devices are shown in Figure 3a and Table 2 for comparison. One of the strong points found

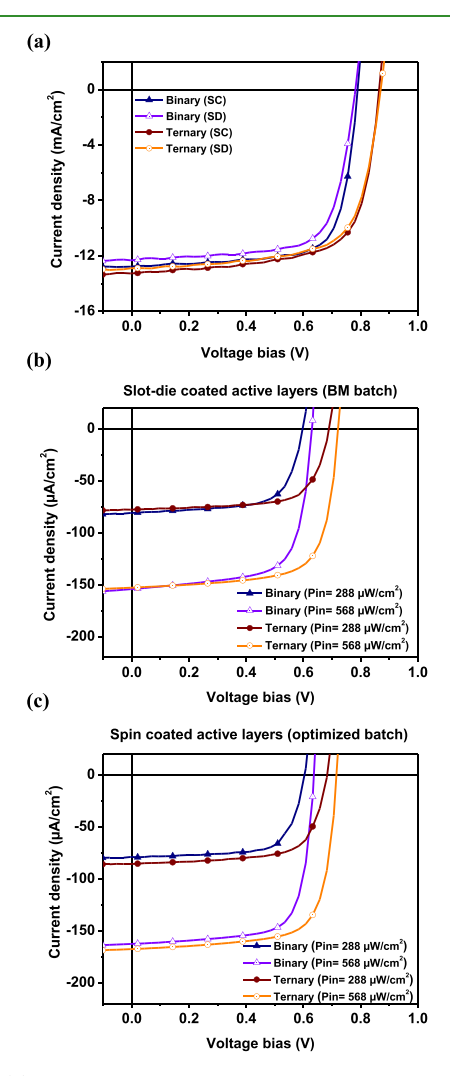


Figure 3. (a) J-V curves of OPV devices SC vs SD with binary and ternary active layers under 1 sun illumination, (b) J-V curves of OPV devices SD with binary and ternary (20 wt % PDI) active layers under different indoor light illuminations, and (c) J-V curves of OPV devices with SC binary and ternary (20 wt % PDI) active layers under different warm indoor light illuminations. ZnO/PEIE was used as the ETL.

in the ternary blend system is that transitioning from spin coating to slot-die coating showed no loss in device performances (PCE of 7.9% for SC devices vs PCE of 7.7% for SD devices). While for the binary devices, there is a PCE loss from 7.4% for SC devices to 6.8% for SD devices, suggesting that the ternary blend is also a more viable system for upscaling. For active layers SD in air and processed from halogen-free solvents, this device performance is the highest for FBT-based OPVs under these conditions so far.

LED Illumination. Next, we examined the OPV devices with SD active layers (binary and ternary) under LED illuminations [ca. 1000 and 2000 lux (288 and 568 μ W/cm²,

Table 2. Photovoltaic Metrics of OPV Devices with SC and SD Binary and Ternary Active Layers under 1 sun Illumination

condition ^{a,b}	$V_{\rm oc} (V)^{\epsilon}$	$J_{\rm sc} ({\rm mA/cm^2})^c$	FF (%) ^c	PCE (%) ^c
SC-binary	0.79 (0.78)	12.7 (12.6)	74 (72)	7.4 (7.1)
SD-binary	0.78 (0.77)	12.3 (12.3)	71 (70)	6.8 (6.7)
SC-ternary	0.86 (0.86)	13.2 (12.9)	69 (69)	7.9 (7.6)
SD-ternary	0.86 (0.86)	12.9 (13.0)	69 (65)	7.7 (7.4)

^aDevice architecture: glass/ITO/ZnO/PEIE/active layer/MoO_x/Ag. ^bDevices processed from o-xylene containing 1% AA additive, 20 mg/ mL total concentration, and (1:1.5) D:A₁:A₂ ratio [D: FBT (Supplied by Brilliant Matters), A₁: PC₆₁BM, and A₂: PDI]. ^cThe values of the best device are reported, while the values in the parentheses stand for the average PCEs from over 15 devices with 0.14 cm² active area. Standard deviation of the PCE values are presented in Figure S2b.

respectively)] with J-V curves shown in Figure 3b and device parameters listed in Table 3. Under low light intensity, the devices with SD ternary active layers exhibited a PCE of 14% with $J_{\rm sc}$ of 153 μ A/cm² and a maximum power density of 79 μ W/cm² (Table S6 and Figure S10 provide photovoltaic parameters of the SC devices under different low light intensities).

As expected at lower light intensities (2000 lux: input power is 568 μ W/cm²), V_{oc} dropped in devices based on both binary (from 0.78 to 0.63 V) and ternary (from 0.86 to 0.72 V) blends compared to the values under 1 sun illumination (Table 2). However, the V_{oc} drop in devices based on ternary blends was compensated by the higher initial V_{oc} values from the PDI contribution which enhanced the overall PCE from 12.0% in the binary to 14.0% in the ternary devices. While all device parameters were enhanced, V_{oc} improvements had the greatest impact on the PCE enabled by the ternary approach.

Utilizing a synthetically optimized batch of the FBT polymer⁴⁷ in the ternary devices (performance under 1 sun illumination is provided in Table S2 and Figure S5), a PCE of 15.5% under 2000 lux illumination (ca. 568 μ W/cm²) is achieved for devices using the SC ternary system compared to 13.1% for the devices based on the binary counterparts, as shown in Figure 3c and Table 3 (Tables S7, S8 and Figures S11, S12 provide photovoltaic parameters of the SC films under different low light intensities). The devices based on SD ternary blends at the optimum conditions achieved output powers of 79.0 and 37.5 μ W/cm² at input powers of 568 and 288 μ W/cm² (ca. 2000 and 1000 lux warm LED light, respectively; Table 3), resulting in PCEs of 14 and 13%, respectively. The devices based on SC ternary blends using the optimized FBT achieved output powers as high as 88 and 42 μ W/cm² at input powers of 568 and 288 μ W/cm² (ca. 2000 and 1000 lux warm LED light, respectively; Table 3). The integrated current density (J_{cal}) was calculated (more details in the Supporting Information, Figure S9) based on the EQE curve of the SC ternary devices and the incident photon flux spectrum (Figure S9a,b, respectively). The integrated current densities (166 μ A/cm²) under warm white LED (2000 lux: input power is 568 μ W/cm²) illumination conditions were found to be consistent with the values from J-V measurements $(167 \mu \text{A/cm}^2)$ which confirmed the reliability of our indoor measurement setup.

In comparison to the literature, the Welch group recently reported a FBT:PC61BM binary system using slot-die coating with a PCE of ~14% (output power of 41 μ W/cm² at input

Table 3. Photovoltaic Metrics of OPV Devices with SC and SD Binary and Ternary Active Layers under Different Warm LED (2700 K) Indoor Light Illumination Intensities ^{a,d}

$P_{\rm in} \left(\mu \rm W/cm^2 \right)$	$V_{\rm oc}$ (V)	$J_{\rm sc} \left(\mu A/{\rm cm}^2 \right)$	FF (%)	PCE (%)	$P_{\rm out} \left(\mu { m W/cm}^2 \right)$	
SD Binary ^b						
288	0.60 (0.60)	80 (79)	68 (67)	11.4 (11.1)	32.7 (31.8)	
568	0.63 (0.63)	154 (147)	70 (68)	12.0 (11.1)	67.9 (63.0)	
		SD Ter	nary ^b			
288	0.69 (0.69)	78 (78)	70 (67)	13.0 (12.5)	37.5 (36.0)	
568	0.72 (0.72)	153 (150)	72 (70)	14.0 (13.3)	79.3 (75.6)	
		SC Bir	nary ^c			
288	0.61 (0.60)	86 (81)	70 (69)	12.8 (11.6)	36.8 (33.5)	
568	0.63 (0.63)	162 (154)	73 (73)	13.1 (12.5)	74.7 (70.8)	
		SC Ter	nary ^c			
288	0.69 (0.68)	87 (84)	70 (69)	14.6 (13.6)	42.1 (39.2)	
568	0.72 (0.72)	167 (159)	73 (71)	15.5 (14.3)	88.0 (81.3)	

^aDevice architecture: glass/ITO/ZnO/PEIE/active layer/MoO_x/Ag. Devices processed from o-xylene containing 1% AA additive, 20 mg/mL total concentration, and (1:1.5) D:A₁:A₂ ratio (D: FBT, A₁: PC₆₁BM, and A₂: PDI). The values of the best device are reported, while the values in the parentheses stand for the average PCEs from over 15 devices with 0.14 cm² active area. ^bFBT supplied by Brilliant Matters. ^cFBT prepared, as described in ref 47. ^dStandard deviation of the PCE values are presented in Figure S2c,d.

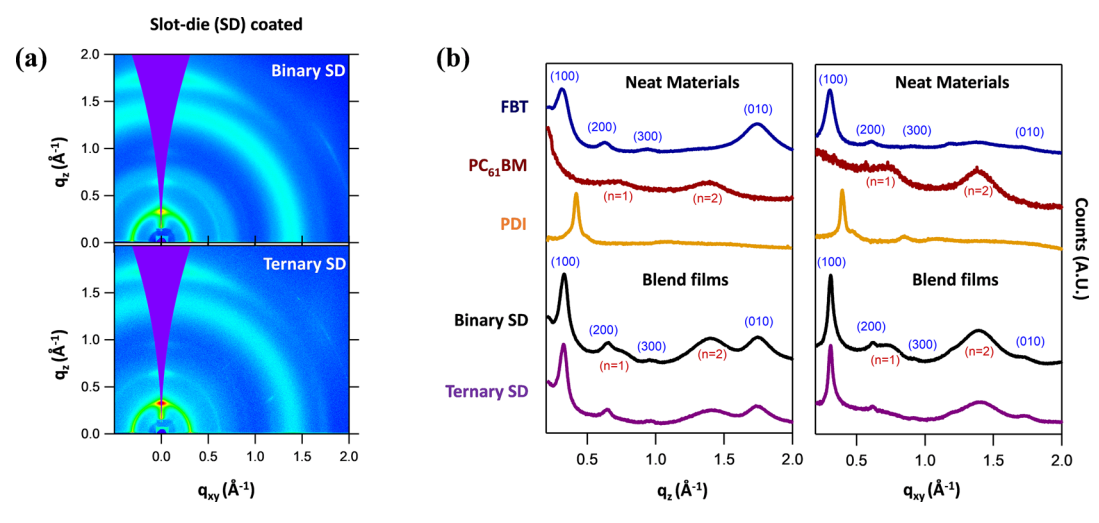


Figure 4. GIWAXS (a) 2D intensity vs q_s -space images for the SD blend films and (b) 1D intensity vs q_s -space (left) and q_{sv} -space (right).

power of 310 μ W/cm²; 1000 lux).⁴⁴ A related FBT:PC₇₁BM binary system, processed via spin coating using halogenated solvents (chlorobenzene), a device PCE of 16% and output power of 45 μ W/cm² at input powers of 280 μ W/cm² (1000 lux) has been achieved.³⁰ A related ternary strategy, where a monomeric PDI acceptor (EP-PDI) was added as a third component to PTB7:PC71BM blends, achieved a device PCE of 15.7% under 500 lux (ca. 170 μ W/cm²) for SC active layers processed from halogenated solvents (chlorobenzene + 3% 1,8diiodooctane).⁵⁶ For this study, we have presented a clear advancement in that not only do PCEs reach 14% using both slot-die coating in air and non-halogenated solvents but also demonstrate higher $V_{\rm oc}$ values of 0.72 V with low $V_{\rm oc}$ losses (<0.17 V) under low light intensities compared to the $V_{\rm oc}$ values of 0.62, 0.59, and 0.65 V reported in the aforementioned studies.

GIWAXS Film Analysis. The intermolecular spacings of semicrystalline regions of the neat donor and acceptor materials as well as the SD blended films were investigated using GIWAXS. Figure 4a shows the 2D detector images for SD binary and ternary blends; complementary 2D detector images for FBT, $PC_{61}BM$, and the PDI are shown in Figures S13–S15. Figure 4b shows the complementary 1D GIWAXS

plots with cake slices in the q_z (out-of-plane, left of Figure 4b) and q_{xy} (in-plane, right of Figure 4b) directions. Table 4 gives

Table 4. Intermolecular Spacings in angstroms of the Semicrystalline Regions in Neat and SD Blend Films from the Peaks of q_x -space in Figure 4b

	d-spacing (Å)						
	FBT			PC ₆₁ BM		PDI	
sample	(100)	(200)	(300)	(010)	(n = 1)	(n = 2)	'
FBT	20.27	9.97	6.68	3.61			
$PC_{61}BM$					8.73	4.52	
PDI							14.96
binary SD	19.04	9.52	6.54	3.61	8.61	4.49	
ternary SD	19.04	9.67	6.54	3.61		4.49	

the relative d-spacings calculated from Figure 4b (left and right), including peak assignments discussed below. Figure S16 and Table S9 in the Supporting Information show the 2D detector images for SC binary and ternary blends and the complementary 1D GIWAXS plots with cake slices in the q_z (out-of-plane).

As shown in Figure 4b, the neat FBT polymer (blue curve) exhibits a lamellar intermolecular spacing in the out-of-plane q_z (100) corresponding to a d-spacing of 20.27 Å, with two higher-order diffraction peaks associated with the (200) and (300) planes. We also observed a peak in the out-of-plane direction that has been attributed to the (010) plane associated with the π - π stacking direction (d-spacing of 3.61Å) by Nguyen et al.²⁸ All peaks were observed in the in-plane direction as well, although at lower intensity, similar to prior reports. PC₆₁BM showed the characteristic isotropic peaks corresponding to d-spacings of 8.73 Å (n = 1) and 4.52 Å (n = 2) which is consistent with previous reports. PDI primarily showed a strong intermolecular spacing of 14.96 Å that was dominant in the out-of-plane direction but also showed isotropic behavior.

The binary blend of FBT:PC₆₁BM, both SD (Figure 4b) and SC (Figure S16b), exhibits the (100), (200), (300), and (010) peaks associated with FBT and the two (n=1,2) isotropic peaks of PC₆₁BM. As listed in Tables 4 and S9, the intermolecular spacings associated with the lamellar stacking direction in FBT are reduced slightly from the neat FBT to the binary blends. This suggests the crystalline presence of both materials but with a closer packed lamellar FBT.

The SD ternary blend (Figure 4) also exhibits the same peaks associated with FBT and PC61BM but there is no evidence of the isotropic 15.31 Å spacing of PDI. The implications of these ternary results are that (i) slot die coating allows enough relaxation time for the materials to crystallize, (ii) PDI intercalates into the FBT and PC₆₁BM and prevents crystallization when SC, and (iii) in slot-die coating leads to FBT and PC₆₁BM segregation from the PDI with enough time for reorganization and forms domains but the PDI remains amorphous. While the GIWAXS data reveal slightly different active layer morphologies owing to the different compositions and processing methods, all PCEs remain similar implying somewhat insensitive bulk heterojunction active layers, which is favorable for upscaling. This is consistent with previous reports of the FBT polymer having thickness-independent performance (PCE of 15.1% achieved under 1000 lux for 500 nm thickness SC active layers).³⁰ The SC ternary blend GIWAXS was inconclusive (Figure S16) as it does not appear to have any notable intermolecular spacing besides a weak FBT (200). Efforts to understand this discrepancy are ongoing, but it does not appear to be due to a surface wetting issue of the substrates used for GIWAXS (Table S10).

Light-Soaking Effect. The light-soaking effect is commonly observed in inverted OPVs with metal oxides as the ETL such as ZnO and TiO2. Devices with these ETLs have to be "activated" for some time by a UV light with photon energies larger than their band gaps $(h\nu > E_g)$ to work properly. In the absence of UV light, poor device performance (particularly FF) with S-shaped J-V curves was obtained.⁵⁸ The OPV device performance enhances gradually upon continuous light illumination (under 1 sun illumination or ultraviolet light) until it reaches a saturation maximum point. The origin of this effect is not yet clear; however, it is generally attributed to the presence of trap sites in the metal-oxide surface that lead to potential barrier between ITO/metal-oxide interface and energy level mismatch at the metal-oxide/active layer interface which seriously limits the device performance. This effect has been shown to be reversible if devices are kept in dark for some time. Several previous reports imply that this effect is quite general. $^{58-62}$ Although we did not observe this effect in our devices under 1 sun illumination, we did observe it under low light LED illumination (Table S11 and Figure S17). The optimized devices based on the ternary blend active layer without light soaking showed a dramatic loss in the FF (40%) under low light intensity (2000 lux) compared to devices with light soaking (FF = 70%). We attributed this effect to the lack of UV portion in the LED source which is needed for devices to work properly. To confirm the hypothesis, we used a 400 nm UV filter (ThorLabs-FGL400S 2" Square GG400 Colored Glass Filter, 400 nm Longpass) during the lightsoaking step to cut the UV portion from 1 sun light. Light soaking with an UV filter resulted in a low FF (44%), similar to the device FF with no light soaking. This effect was observed in all devices with the ZnO ETL (Table S12 and Figure S18). Although PEIE as the ETL (ITO/PEIE/binary active layer/ MoO_x/Ag) did not require the light-soaking step, it showed much lower performance (PCE = 10.3%) compared to ZnO and ZnO/PEIE interlayers (PCE = 12%) (Table S11 and Figure S17). Efforts to find efficient and light-soaking-free alternatives for the ETL under low light intensities are promising. Tin oxide (SnO₂) has previously been reported as efficient replacement for light-soaking-free ETL under 1 sun illumination.⁵⁸ A recent study showed that the SnO₂ ETL can efficiently replace ZnO ETL to avoid an additional lightsoaking step for indoor applications.⁶³ Under LED illumination (1000 lux), the authors reported 9.7% with ZnO compared to 12.7% with SnO₂ for small size devices and 10.7% with ZnO compared to 13% with SnO₂ for module size devices based on a flexible device architecture: PET/ITO/ SnO₂/PV2001:PCBM/PEDOT:PSS/silver grid. These results along with our results confirm the need to find alternatives for ZnO ETL for efficient OPV devices under low light intensities.

Device Stability. Stability of OPVs is a key issue toward the transition from lab to fab. In this study, we investigated the stability of the devices with SD ternary blend active layers under different conditions. Three similar sets of devices have been prepared and examined under three different conditions (more details are provided in the Supporting Information, page S24): (1) an inert atmosphere in a nitrogen-filled glovebox, (2) ambient conditions at room temperature and 30% relative humidity, and (3) thermal stress in a nitrogen-filled glovebox under continuous heating at 80 °C. All devices were unencapsulated and kept under dark conditions. OPV device lifetime is usually given by the Ts80 factor which is defined by the point at which the PCEs drop to 80% of its stabilized value after the burn-in deterioration. Figure 5a shows the normalized device parameters. We conducted this stability test over the course of 500 h at regular intervals. The performance reached 80% of its initial value after 500 h for devices kept in a nitrogen-filled glovebox. However, the devices under ambient conditions reach the same value after 300 h, as shown in Figure 5b. Devices exposed to thermal stress exhibited a quite different degradation trend. After the first 30 min heating, the PCEs drop to 78% of its initial value. After that burn-in period, devices showed a stable trend. PCEs after 300 h thermal cycles drop to 71% of the initial value (93% of its value after the burn-in) which shows the high thermal stability of the devices with the ternary approach. The ternary blend in this study showed higher stability compared to previous studies that reported about FBT:PC₇₁BM stability under thermal stress. ^{28,29} The ternary approach in OPVs has previously been shown to have a positive impact on the morphological stability of the active layers under thermal stress

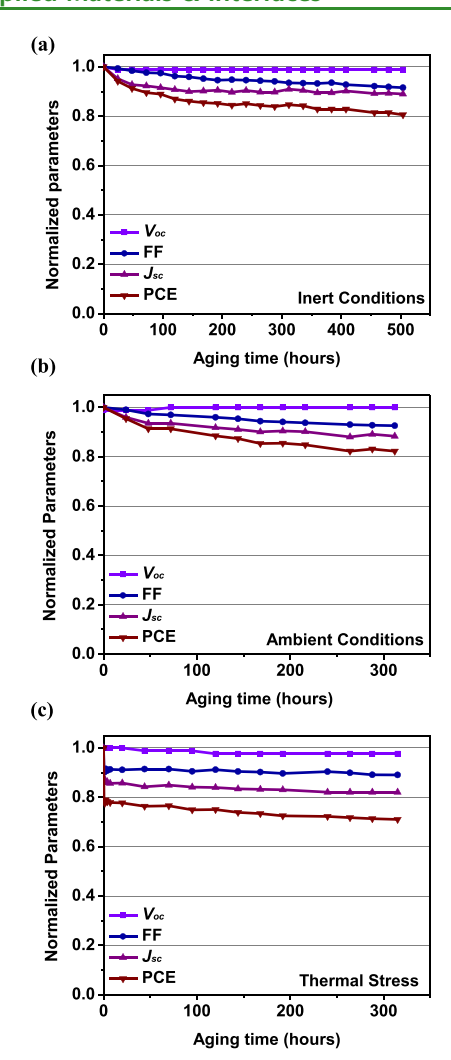


Figure 5. Normalized parameters of the unencapsulated inverted OPV devices based on SD optimized ternary active layers (FBT/PC $_{61}$ BM/PDI; 1:1.2:0.3) representing the stability tests under (a) inert conditions in a nitrogen-filled glovebox, (b) ambient conditions at room temperature and 30% relative humidity (R.H.), and (c) thermal stress with continuous heating at 80 °C in a nitrogen-filled glovebox. All devices are unencapsulated and tested in air under 1 sun illumination. ZnO/PEIE was used as the ETL.

enhancing the overall device stability which is consistent with our findings. 51,66,67

CONCLUSIONS

Efficient ternary-based OPVs have been successfully SD in air from halogen-free solvents and tested for indoor light harvesting. Optimized ternary systems composed of FBT (polymer donor), PC₆₁BM (fullerene acceptor), and PDI (NFA) resulted in a device PCE of 14.0% and a maximum power density of 79 μ W/cm² under low light intensities. The binary (FBT:PC₆₁BM) SD counterparts achieved PCE of 12.0% and a maximum power density of 68 μ W/cm² under the same illumination conditions. SC devices from an optimized FBT batch showed a PCE of 15.5% and a maximum power density of 88 μ W/cm². Using slot-die coating and environmentally friendly solvents to fabricate efficient devices is an important step toward scalable iOPVs. This work paves the way toward large-area efficient OPVs for indoor light recycling applications.

ASSOCIATED CONTENT

Supporting Information

The Supporting Information is available free of charge at https://pubs.acs.org/doi/10.1021/acsami.0c11809.

J-V curves of the binary devices, AFM and PL of binary versus ternary films, J-V curves of SC binary and ternary devices, indoor testing setup calibration details, J-V curves of SC and SD under low light intensity, GIWAXS (1D, 2D), contact angle measurements, and light-soaking effect under various conditions (PDF)

AUTHOR INFORMATION

Corresponding Authors

Erin L. Ratcliff — Department of Materials Science and Engineering, Department of Chemical and Environmental Engineering, and Department of Chemistry and Biochemistry, University of Arizona, Tucson, Arizona 85721, United States; orcid.org/0000-0002-2360-8436; Email: ratcliff@email.arizona.edu

Gregory C. Welch — Department of Chemistry, University of Calgary, Calgary, Alberta T2N 1N4, Canada; oorcid.org/0000-0002-3768-937X; Email: gregory.welch@ucalgary.ca

Authors

Mahmoud E. Farahat — Department of Chemistry, University of Calgary, Calgary, Alberta T2N 1N4, Canada; orcid.org/0000-0002-0547-1296

Audrey Laventure — Department of Chemistry, University of Calgary, Calgary, Alberta T2N 1N4, Canada; ⊚ orcid.org/ 0000-0002-0867-0231

Michael A. Anderson – Department of Materials Science and Engineering, University of Arizona, Tucson, Arizona 85721, United States

Mathieu Mainville – Department of Chemistry, Université Laval, Quebec City, Quebec GIV 0A6, Canada

Francesco Tintori — Department of Chemistry, University of Calgary, Calgary, Alberta T2N 1N4, Canada

Mario Leclerc — Department of Chemistry, Université Laval, Quebec City, Quebec G1V 0A6, Canada; orcid.org/0000-0003-2458-9633

Complete contact information is available at: https://pubs.acs.org/10.1021/acsami.0c11809

Notes

The authors declare the following competing financial interest(s): Work is covered under a USTPO provisonal patent. Number: 63/079,147. Filing date: September 16, 2020.

ACKNOWLEDGMENTS

G.C.W. acknowledges the Canada Research Chairs Program, CFI JELF (34102), NSERC Engage Plus (537557-18), and the University of Calgary. Brilliant Matters is thanked for materials' donation and financial support. All authors acknowledge and thank Dr. Sergey Dayneko for the help provided in calculations and calibration of the indoor testing equipment and Edward Cieplechowicz for the synthesis of tPDI₂N-EH. Dr. Philippe Berrouard, Dr. François Grenier, and Dr. Jean-Rémi Pouliot from Brilliant Matters (QC, Canada) are thanked for helpful discussions and Dr. Jonas Bergqvist and Dr. Thomas Österberg from Epishine (Sweden) for discussion and insight on testing OPVs under LED light. This research was undertaken thanks in part to funding from the Canada First Research Excellence

Fund (CFREF). A.L. acknowledges NSERC for a postdoctoral fellowship. M.L. also thanks NSERC for supporting this work. A portion of this work is supported by the National Science Foundation under grant award DMR-1608289. M.A.A. was supported by the National Science Foundation under grant award DGE-1735173. Use of the SSRL, SLAC National Accelerator Laboratory, is supported by the U.S. Department of Energy, Office of Science, Office of Basic Energy Sciences under contract no. DE-AC02-76SF00515.

REFERENCES

- (1) Mathews, I.; Kantareddy, S. N.; Buonassisi, T.; Peters, I. M. Technology and Market Perspective for Indoor Photovoltaic Cells. *Joule* **2019**, *3*, 1415–1426.
- (2) Chen, F.-C. Emerging Organic and Organic/Inorganic Hybrid Photovoltaic Devices for Specialty Applications: Low-Level-Lighting Energy Conversion and Biomedical Treatment. *Adv. Opt. Mater.* **2019**, *7*, 1800662.
- (3) Cutting, C. L.; Bag, M.; Venkataraman, D. Indoor Light Recycling: A New Home for Organic Photovoltaics. *J. Mater. Chem. C* **2016**, *4*, 10367–10370.
- (4) Raj, A.; Steingart, D. Review—Power Sources for the Internet of Things. *J. Electrochem. Soc.* **2018**, *165*, B3130.
- (5) Steim, R.; Ameri, T.; Schilinsky, P.; Waldauf, C.; Dennler, G.; Scharber, M.; Brabec, C. J. Organic Photovoltaics for Low Light Applications. *Sol. Energy Mater. Sol. Cells* **2011**, *95*, 3256–3261.
- (6) Freitag, M.; Teuscher, J.; Saygili, Y.; Zhang, X.; Giordano, F.; Liska, P.; Hua, J.; Zakeeruddin, S. M.; Moser, J.-E.; Grätzel, M.; Hagfeldt, A. Dye-Sensitized Solar Cells for Efficient Power Generation under Ambient Lighting. *Nat. Photonics* **2017**, *11*, 372–378.
- (7) Chen, C.-Y.; Lee, W.-H.; Hsiao, S.-Y.; Tsai, W.-L.; Yang, L.; Lin, H.-L.; Chou, H.-J.; Lin, H.-W. Vacuum-Deposited Perovskite Photovoltaics for Highly Efficient Environmental Light Energy Harvesting. J. Mater. Chem. A 2019, 7, 3612–3617.
- (8) Chen, C.-Y.; Chang, J.-H.; Chiang, K.-M.; Lin, H.-L.; Hsiao, S.-Y.; Lin, H.-W. Perovskite Photovoltaics for Dim-Light Applications. *Adv. Funct. Mater.* **2015**, *25*, 7064–7070.
- (9) Ding, Z.; Zhao, R.; Yu, Y.; Liu, J. All-Polymer Indoor Photovoltaics with High Open-Circuit Voltage. *J. Mater. Chem. A* **2019**, *7*, 26533–26539.
- (10) Zhou, Y.; Khan, T. M.; Shim, J. W.; Dindar, A.; Fuentes-Hernandez, C.; Kippelen, B. All-Plastic Solar Cells with a High Photovoltaic Dynamic Range. *J. Mater. Chem. A* **2014**, *2*, 3492–3497.
- (11) Yang, S.-S.; Hsieh, Z.-C.; Keshtov, M. L.; Sharma, G. D.; Chen, F.-C. Toward High-Performance Polymer Photovoltaic Devices for Low-Power Indoor Applications. *Sol. RRL* **2017**, *1*, 1700174.
- (12) Lee, H. K. H.; Wu, J.; Barbé, J.; Jain, S. M.; Wood, S.; Speller, E. M.; Li, Z.; Castro, F. A.; Durrant, J. R.; Tsoi, W. C. Organic Photovoltaic Cells Promising Indoor Light Harvesters for Self-Sustainable Electronics. *J. Mater. Chem. A* **2018**, *6*, 5618—5626.
- (13) Cui, Y.; Yao, H.; Zhang, J.; Xian, K.; Zhang, T.; Hong, L.; Wang, Y.; Xu, Y.; Ma, K.; An, C.; He, C.; Wei, Z.; Gao, F.; Hou, J. Single-Junction Organic Photovoltaic Cells with Approaching 18% Efficiency. *Adv. Mater.* **2020**, *32*, 1908205.
- (14) Farahat, M. E.; Perumal, P.; Budiawan, W.; Chen, Y.-F.; Lee, C.-H.; Chu, C.-W. Efficient Molecular Solar Cells Processed from Green Solvent Mixtures. *J. Mater. Chem. A* **2017**, *5*, 571–582.
- (15) Zhang, S.; Ye, L.; Zhang, H.; Hou, J. Green-Solvent-Processable Organic Solar Cells. *Mater. Today* **2016**, *19*, 533–543.
- (16) Søndergaard, R.; Hösel, M.; Angmo, D.; Larsen-Olsen, T. T.; Krebs, F. C. Roll-to-Roll Fabrication of Polymer Solar Cells. *Mater. Today* **2012**, *15*, 36–49.
- (17) Maisch, P.; Tam, K. C.; Schilinsky, P.; Egelhaaf, H.-J.; Brabec, C. J. Shy Organic Photovoltaics: Digitally Printed Organic Solar Modules With Hidden Interconnects. *Sol. RRL* **2018**, *2*, 1800005.
- (18) Blankenburg, L.; Schultheis, K.; Schache, H.; Sensfuss, S.; Schrödner, M. Reel-to-Reel Wet Coating as an Efficient up-Scaling

- Technique for the Production of Bulk-Heterojunction Polymer Solar Cells. Sol. Energy Mater. Sol. Cells 2009, 93, 476–483.
- (19) Carlé, J. E.; Andersen, T. R.; Helgesen, M.; Bundgaard, E.; Jørgensen, M.; Krebs, F. C. A Laboratory Scale Approach to Polymer Solar Cells Using One Coating/Printing Machine, Flexible Substrates, No ITO, No Vacuum and No Spincoating. *Sol. Energy Mater. Sol. Cells* **2013**, *108*, 126–128.
- (20) Lucera, L.; Machui, F.; Kubis, P.; Schmidt, H. D.; Adams, J.; Strohm, S.; Ahmad, T.; Forberich, K.; Egelhaaf, H.-J.; Brabec, C. J. Highly Efficient, Large Area, Roll Coated Flexible and Rigid OPV Modules with Geometric Fill Factors up to 98.5% Processed with Commercially Available Materials. *Energy Environ. Sci.* **2016**, *9*, 89–94.
- (21) Ryu, H. S.; Park, S. Y.; Lee, T. H.; Kim, J. Y.; Woo, H. Y. Recent Progress in Indoor Organic Photovoltaics. *Nanoscale* **2020**, *12*, 5792–5804.
- (22) Mainville, M.; Leclerc, M. Recent Progress on Indoor Organic Photovoltaics: From Molecular Design to Production Scale. *ACS Energy Lett.* **2020**, *5*, 1186–1197.
- (23) Goo, J. S.; Lee, J.-H.; Shin, S.-C.; Park, J.-S.; Shim, J. W. Undoped ZnO Electrodes for Low-Cost Indoor Organic Photovoltaics. J. Mater. Chem. A 2018, 6, 23464–23472.
- (24) Cui, Y.; Wang, Y.; Bergqvist, J.; Yao, H.; Xu, Y.; Gao, B.; Yang, C.; Zhang, S.; Inganäs, O.; Gao, F.; Hou, J. Wide-Gap Non-Fullerene Acceptor Enabling High-Performance Organic Photovoltaic Cells for Indoor Applications. *Nat. Energy* **2019**, *4*, 768–775.
- (25) Lechêne, B. P.; Cowell, M.; Pierre, A.; Evans, J. W.; Wright, P. K.; Arias, A. C. Organic Solar Cells and Fully Printed Super-Capacitors Optimized for Indoor Light Energy Harvesting. *Nano Energy* **2016**, *26*, 631–640.
- (26) Aoki, Y. Photovoltaic Performance of Organic Photovoltaics for Indoor Energy Harvester. *Org. Electron.* **2017**, *48*, 194–197.
- (27) Ho, J. K. W.; Yin, H.; Kong So, S. From 33% to 57% an Elevated Potential of Efficiency Limit for Indoor Photovoltaics. *J. Mater. Chem. A* **2020**, *8*, 1717–1723.
- (28) Nguyen, T. L.; Choi, H.; Ko, S.-J.; Uddin, M. A.; Walker, B.; Yum, S.; Jeong, J.-E.; Yun, M. H.; Shin, T. J.; Hwang, S.; Kim, J. Y.; Woo, H. Y. Semi-Crystalline Photovoltaic Polymers with Efficiency Exceeding 9% in a ~300 Nm Thick Conventional Single-Cell Device. *Energy Environ. Sci.* **2014**, *7*, 3040–3051.
- (29) Song, S.; Lee, K. T.; Koh, C. W.; Shin, H.; Gao, M.; Woo, H. Y.; Vak, D.; Kim, J. Y. Hot Slot Die Coating for Additive-Free Fabrication of High Performance Roll-to-Roll Processed Polymer Solar Cells. *Energy Environ. Sci.* **2018**, *11*, 3248–3255.
- (30) Shin, S.-C.; Koh, C. W.; Vincent, P.; Goo, J. S.; Bae, J.-H.; Lee, J.-J.; Shin, C.; Kim, H.; Woo, H. Y.; Shim, J. W. Ultra-Thick Semi-Crystalline Photoactive Donor Polymer for Efficient Indoor Organic Photovoltaics. *Nano Energy* **2019**, *58*, 466–475.
- (31) Gasparini, N.; Salleo, A.; McCulloch, I.; Baran, D. The Role of the Third Component in Ternary Organic Solar Cells. *Nat. Rev. Mater.* **2019**, *4*, 229–242.
- (32) Lu, L.; Xu, T.; Chen, W.; Landry, E. S.; Yu, L. Ternary Blend Polymer Solar Cells with Enhanced Power Conversion Efficiency. *Nat. Photonics* **2014**, *8*, 716–722.
- (33) Cheng, P.; Zhan, X. Versatile Third Components for Efficient and Stable Organic Solar Cells. *Mater. Horiz.* **2015**, 2, 462–485.
- (34) Xiao, L.; He, B.; Hu, Q.; Maserati, L.; Zhao, Y.; Yang, B.; Kolaczkowski, M. A.; Anderson, C. L.; Borys, N. J.; Klivansky, L. M.; Chen, T. L.; Schwartzberg, A. M.; Russell, T. P.; Cao, Y.; Peng, X.; Liu, Y. Multiple Roles of a Non-Fullerene Acceptor Contribute Synergistically for High-Efficiency Ternary Organic Photovoltaics. *Joule* 2018, 2, 2154–2166.
- (35) Chen, Y.; Ye, P.; Jia, X.; Gu, W.; Xu, X.; Wu, X.; Wu, J.; Liu, F.; Zhu, Z.-G.; Huang, H. Tuning Voc for High Performance Organic Ternary Solar Cells with Non-Fullerene Acceptor Alloys. *J. Mater. Chem. A* 2017, *5*, 19697–19702.
- (36) Cho, Y.; Kumari, T.; Jeong, S.; Lee, S. M.; Jeong, M.; Lee, B.; Oh, J.; Zhang, Y.; Huang, B.; Chen, L.; Yang, C. Guest-Oriented Non-Fullerene Acceptors for Ternary Organic Solar Cells with over 16.0%

- and 22.7% Efficiencies under One-Sun and Indoor Light. *Nano Energy* **2020**, 75, 104896.
- (37) Bai, Y.; Yu, R.; Bai, Y.; Zhou, E.; Hayat, T.; Alsaedi, A.; Tan, Z. Ternary Blend Strategy in Benzotriazole-Based Organic Photovoltaics for Indoor Application. *Green Energy Environ.* **2020**, DOI: 10.1016/j.gee.2020.07.017.
- (38) Singh, R.; Duan, T.; Kan, Z.; Chochos, C. L.; Kini, G. P.; Kumar, M.; Park, J.; Lee, J.; Lee, J.-J. Revealing the Structural Effects of Non-Fullerene Acceptors on the Performances of Ternary Organic Photovoltaics under Indoor Light Conditions. *Nano Energy* **2020**, 75, 104934
- (39) Dayneko, S. V.; Hendsbee, A. D.; Welch, G. C. Combining Facile Synthetic Methods with Greener Processing for Efficient Polymer-Perylene Diimide Based Organic Solar Cells. *Small Methods* **2018**, *2*, 1800081.
- (40) Tintori, F.; Laventure, A.; Welch, G. C. Perylene Diimide Based Organic Photovoltaics with Slot-Die Coated Active Layers from Halogen-Free Solvents in Air at Room Temperature. ACS Appl. Mater. Interfaces 2019, 11, 39010–39017.
- (41) Laventure, A.; Harding, C. R.; Cieplechowicz, E.; Li, Z.; Wang, J.; Zou, Y.; Welch, G. C. Screening Quinoxaline-Type Donor Polymers for Roll-to-Roll Processing Compatible Organic Photovoltaics. ACS Appl. Polym. Mater. 2019, 1, 2168–2176.
- (42) Abd-Ellah, M.; Cann, J.; Dayneko, S. V.; Laventure, A.; Cieplechowicz, E.; Welch, G. C. Interfacial ZnO Modification Using a Carboxylic Acid Functionalized N-Annulated Perylene Diimide for Inverted Type Organic Photovoltaics. *ACS Appl. Electron. Mater.* **2019**, *1*, 1590–1596.
- (43) Dayneko, S. V.; Hendsbee, A. D.; Cann, J. R.; Cabanetos, C.; Welch, G. C. Ternary Organic Solar Cells: Using Molecular Donor or Acceptor Third Components to Increase Open Circuit Voltage. *New J. Chem.* **2019**, *43*, 10442–10448.
- (44) Dayneko, S. V.; Pahlevani, M.; Welch, G. C. Indoor Photovoltaics: Photoactive Material Selection, Greener Ink Formulations, and Slot-Die Coated Active Layers. *ACS Appl. Mater. Interfaces* **2019**, *11*, 46017–46025.
- (45) Lee, M. H. A Machine Learning—Based Design Rule for Improved Open-Circuit Voltage in Ternary Organic Solar Cells. *Adv. Intell. Syst.* **2020**, *2*, 1900108.
- (46) Sprau, C.; Buss, F.; Wagner, M.; Landerer, D.; Koppitz, M.; Schulz, A.; Bahro, D.; Schabel, W.; Scharfer, P.; Colsmann, A. Highly Efficient Polymer Solar Cells Cast from Non-Halogenated Xylene/Anisaldehyde Solution. *Energy Environ. Sci.* **2015**, *8*, 2744–2752.
- (47) Mainville, M.; Tremblay, V.; Fenniri, M. Z.; Laventure, A.; Farahat, M. E.; Ambrose, R.; Welch, G. C.; Hill, I. G.; Leclerc, M. Water Compatible Direct (Hetero)Arylation Polymerization of PPDT2FBT: A Pathway Towards Large-Scale Production of Organic Solar Cells. *Asian J. Org. Chem.* 2020, DOI: 10.1002/ajoc.202000231.
- (48) Hendsbee, A. D.; Sun, J.-P.; Law, W. K.; Yan, H.; Hill, I. G.; Spasyuk, D. M.; Welch, G. C. Synthesis, Self-Assembly, and Solar Cell Performance of N-Annulated Perylene Diimide Non-Fullerene Acceptors. *Chem. Mater.* **2016**, *28*, 7098–7109.
- (49) Sun, Y.; Seo, J. H.; Takacs, C. J.; Seifter, J.; Heeger, A. J. Inverted Polymer Solar Cells Integrated with a Low-Temperature-Annealed Sol-Gel-Derived ZnO Film as an Electron Transport Layer. *Adv. Mater.* **2011**, *23*, 1679–1683.
- (50) Oosterhout, S. D.; Savikhin, V.; Zhang, J.; Zhang, Y.; Burgers, M. A.; Marder, S. R.; Bazan, G. C.; Toney, M. F. Mixing Behavior in Small Molecule:Fullerene Organic Photovoltaics. *Chem. Mater.* **2017**, 29, 3062–3069.
- (51) Landerer, D.; Mertens, A.; Freis, D.; Droll, R.; Leonhard, T.; Schulz, A. D.; Bahro, D.; Colsmann, A. Enhanced Thermal Stability of Organic Solar Cells Comprising Ternary D-D-A Bulk-Heterojunctions. *npj Flexible Electron.* **2017**, *1*, 11.
- (52) Vespa, M.; Cann, J. R.; Dayneko, S. V.; Melville, O. A.; Hendsbee, A. D.; Zou, Y.; Lessard, B. H.; Welch, G. C. Synthesis of a Perylene Diimide Dimer with Pyrrolic N–H Bonds and N-Functionalized Derivatives for Organic Field-Effect Transistors and Organic Solar Cells. Eur. J. Org. Chem. 2018, 2018, 4592–4599.

- (53) Srivastava, S. B.; Srivastava, S. K.; Singh, S. P. Molecular-Shape-Induced Efficiency Enhancement in $PC_{61}BM$ and $PC_{71}BM$ Based Ternary Blend Organic Solar Cells. *J. Phys. Chem. C* **2017**, *121*, 17104–17111.
- (54) Kang, H.; Uddin, M. A.; Lee, C.; Kim, K.-H.; Nguyen, T. L.; Lee, W.; Li, Y.; Wang, C.; Woo, H. Y.; Kim, B. J. Determining the Role of Polymer Molecular Weight for High-Performance All-Polymer Solar Cells: Its Effect on Polymer Aggregation and Phase Separation. *J. Am. Chem. Soc.* **2015**, *137*, 2359–2365.
- (55) Jin, W.-Y.; Ginting, R. T.; Jin, S.-H.; Kang, J.-W. Highly Stable and Efficient Inverted Organic Solar Cells Based on Low-Temperature Solution-Processed PEIE and ZnO Bilayers. *J. Mater. Chem. A* **2016**, *4*, 3784–3791.
- (56) Singh, R.; Shin, S.-C.; Lee, H.; Kim, M.; Shim, J. W.; Cho, K.; Lee, J.-J. Ternary Blend Strategy for Achieving High-Efficiency Organic Photovoltaic Devices for Indoor Applications. *Chem.—Eur. J.* **2019**, 25, 6154–6161.
- (57) Verploegen, E.; Miller, C. E.; Schmidt, K.; Bao, Z.; Toney, M. F. Manipulating the Morphology of P3HT–PCBM Bulk Heterojunction Blends with Solvent Vapor Annealing. *Chem. Mater.* **2012**, 24, 3923–3931.
- (58) Trost, S.; Behrendt, A.; Becker, T.; Polywka, A.; Görrn, P.; Riedl, T. Tin Oxide (SnOx) as Universal "Light-Soaking" Free Electron Extraction Material for Organic Solar Cells. *Adv. Energy Mater.* **2015**, 5, 1500277.
- (59) Trost, S.; Zilberberg, K.; Behrendt, A.; Polywka, A.; Görrn, P.; Reckers, P.; Maibach, J.; Mayer, T.; Riedl, T. Overcoming the "Light-Soaking" Issue in Inverted Organic Solar Cells by the Use of Al:ZnO Electron Extraction Layers. *Adv. Energy Mater.* **2013**, *3*, 1437–1444.
- (60) Yan, Y.; Cai, F.; Yang, L.; Li, J.; Zhang, Y.; Qin, F.; Xiong, C.; Zhou, Y.; Lidzey, D. G.; Wang, T. Light-Soaking-Free Inverted Polymer Solar Cells with an Efficiency of 10.5% by Compositional and Surface Modifications to a Low-Temperature-Processed TiO2 Electron-Transport Layer. *Adv. Mater.* **2017**, *29*, 1604044.
- (61) Prosa, M.; Tessarolo, M.; Bolognesi, M.; Margeat, O.; Gedefaw, D.; Gaceur, M.; Videlot-Ackermann, C.; Andersson, M. R.; Muccini, M.; Seri, M.; Ackermann, J. Enhanced Ultraviolet Stability of Air-Processed Polymer Solar Cells by Al Doping of the ZnO Interlayer. ACS Appl. Mater. Interfaces 2016, 8, 1635–1643.
- (62) Cowan, S. R.; Schulz, P.; Giordano, A. J.; Garcia, A.; MacLeod, B. A.; Marder, S. R.; Kahn, A.; Ginley, D. S.; Ratcliff, E. L.; Olson, D. C. Chemically Controlled Reversible and Irreversible Extraction Barriers Via Stable Interface Modification of Zinc Oxide Electron Collection Layer in Polycarbazole-Based Organic Solar Cells. *Adv. Funct. Mater.* 2014, 24, 4671–4680.
- (63) Ylikunnari, M.; Välimäki, M.; Väisänen, K.-L.; Kraft, T. M.; Sliz, R.; Corso, G.; Po, R.; Barbieri, R.; Carbonera, C.; Gorni, G.; Vilkman, M. Flexible OPV Modules for Highly Efficient Indoor Applications. *Flexible Printed Electron.* **2020**, *5*, 014008.
- (64) Zhang, Y.; Samuel, I. D. W.; Wang, T.; Lidzey, D. G. Current Status of Outdoor Lifetime Testing of Organic Photovoltaics. *Adv. Sci.* **2018**, *5*, 1800434.
- (65) Kang, H.; Kim, G.; Kim, J.; Kwon, S.; Kim, H.; Lee, K. Bulk-Heterojunction Organic Solar Cells: Five Core Technologies for Their Commercialization. *Adv. Mater.* **2016**, 28, 7821–7861.
- (66) Kim, T.; Choi, J.; Kim, H. J.; Lee, W.; Kim, B. J. Comparative Study of Thermal Stability, Morphology, and Performance of All-Polymer, Fullerene—Polymer, and Ternary Blend Solar Cells Based on the Same Polymer Donor. *Macromolecules* **2017**, *50*, 6861–6871.
- (67) Dong, Y.; Zou, Y.; Yuan, J.; Yang, H.; Wu, Y.; Cui, C.; Li, Y. Ternary Polymer Solar Cells Facilitating Improved Efficiency and Stability. *Adv. Mater.* **2019**, *31*, No. e1904601.